Available online at www.sciencedirect.com

ScienceDirect

Advances in Space Research xxx (2020) xxx–xxx

ADVANCES IN SPACE RESEARCH (a COSPAR publication)

www.elsevier.com/locate/asr

Solar sail deployment dynamics ☆

Behrad Vatankhahghadim *, Christopher J. Damaren

University of Toronto Institute for Aerospace Studies, 4925 Dufferin Street, Toronto, Ontario M3H 5T6, Canada

Received 8 January 2020; received in revised form 12 March 2020; accepted 23 March 2020

Abstract

The deployment dynamics of a solar sail consisting of four flexible booms and four membrane quadrants are studied. First, previous work on modelling only one membrane quadrant attached to two axially moving beams using time-varying quasi-modal expansion is extended to be applicable to the complete four-quadrant system. This is achieved via "lifting" the quadrant-level matrices into system-level forms by mapping the former's constituent blocks to the correct partitions in the latter. After the quadrant-to-system conversion of the matrices, the equations of motion from the authors' previous work readily apply to the complete system. Modal analysis is performed on a constant-length sail to validate the model's basic foundations against the results obtained by finite element methods in the past literature. Deployment simulation results are presented, numerical parameter studies that show possibility of instability are performed using the system's eigenvalues, and the stability results are discussed.

Keywords: Solar sails; Beam-membrane vibrations; Axially translating continua; Deployment dynamics and stability

1. Introduction

Translating continua of constant or time-varying length find applications in many areas of engineering, such as magnetic tapes, elevator cables, robotic arms, the paper industry, and spacecraft antennas. Surveys of some of the early works in such areas were presented in Mote (1972), Wickert and Mote (1988), and more recent efforts were reviewed in Zhu (2000). In the context of spacecraft, deployment was examined in Hedgepeth (1970), Cloutier (1968), Cherchas (1971), Hughes (1972), among others. More generally, studies on axially translating strings, considered to be among the simplest of translating continua that lead to second-order equations, can be traced back to Carrier (1949), Sack (1954), Miranker (1960). Transverse vibration of axially translating beams, described by fourth-order systems, was studied in Leech (1970), Tabarrok et al. (1974), Wang and Wei (1987), Wang and Wei (1994), Wang et al. (2009), Yang et al. (2016), among others, in which "quasi-modal expansion" using the eigenfunctions of a cantilevered beam was used on the deflections, similarly to Cherchas and Gossain (1974), Hughes (1976), Janković (1979) for spacecraft applications. In addition, the out-of-plane dynamics of translating membranes were examined in Niemi and Pramila (1987), Koivurova and Pramila (1997), Shin et al. (2005).

Focusing on the dynamics of coupled multibody systems, most relevant past works include Hughes and Garg (1973), Shaker (1976), Weeks (1986), which also make use of the quasi-modal approach, but only after expressing the deflections of solar panels in terms of those of their

☆ An early version of this paper was previously presented in Vatankhahghadim and Damaren (2018). Notable revisions include updated simulation results that better align with the assumptions, an extended literature survey, additions and omissions for clarity and conciseness, as well as attempts to offer physical explanations for the results.

* Corresponding author.
E-mail addresses: behrad.vatankhahghadim@mail.utoronto.ca (B. Vatankhahghadim), damaren@utias.utoronto.ca (C.J. Damaren).

https://doi.org/10.1016/j.asr.2020.03.029
0273-1177/

support booms. In a similar manner, the out-of-plane deflections of a single solar sail quadrant was examined in Vatankhahghadim and Damaren (2019), in which analytic expressions for the rate of change of vibration energy, resembling those in Zhu and Ni (2000), Wang et al. (2009) for deploying beams, were also obtained.

Heavily numerical approaches have been used to study solar sail deployment dynamics, such as in Shirasawa et al. (2011), replacing finite elements with masses, springs, and dampers; and in Zhao et al. (2013), Tian et al. (2015), using a global coordinate system. Abandoning simple analytical models, Sakamoto et al. (2011) developed a geometrically nonlinear finite element method (FEM), and proposed elements with variable properties. Earlier works on translating beams and membranes that also used FEM include Stylianou and Tabarrok (1994,) and Niemi and Pramila (1987), Koivurova and Pramila (1997), respectively. Ground-based deployment experiments have been performed, for example in Block et al. (2011), Spröwitz et al. (2018), using coilable carbonfiber-reinforced plastic booms and Upilex-S® or Mylar® films, which are the structures of interest in this document. Measurement data are available in Spröwitz et al. (2018), Wong and Pellegrino (2006), Pappa et al. (2006) for constant-length cases, obtained via strain gauges on the booms or using digital image correlation.

A natural and important question that arises in the context of deployable structures is that of stability. Translating continua of varying length could be classified as non-conservative gyroscopic systems (Stylianou and Tabarrok, 1994). For such systems, static methods such as those seeking the appearance of non-trivial equilibria may yield results that are inconsistent with the more reliable ones furnished by the kinetic (vibration) methods (Ziegler, 1977). In the past, the stability of translating materials has been studied by examining the transverse displacements' boundedness, such as in Wickert and Mote (1990), Stylianou and Tabarrok (1994), Lin (1997), Zhu (2000), as well as from an energy viewpoint, such as in Miranker (1960), Wickert and Mote (1989), Zhu and Ni (2000), Zhu (2000). In Vatankhahghadim and Damaren (2019), it was shown that the transverse vibration energy of the hybrid beam-membrane system of a solar sail monotonically decreases and increases during deployment and retraction, respectively. Similarly to the observations in Zhu and Ni (2000), Wang et al. (2009), however, this elegant conclusion does not guarantee boundedness of displacements during extension.

A primary contribution of this document is to build upon Vatankhahghadim and Damaren (2019) and numerically investigate the possibility of divergence using a kinetic approach, and study the effects of pretension and deployment rate on the onset of such phenomena. Whereas the formulation of Vatankhahghadim and Damaren (2019) focused on a single sail quadrant, the present document provides more details on a complete and more realistic model of a solar sail, namely one with four axially translating beams, with four thin membrane quadrants attached in-between. New stability results pertinent to the complete sail's behaviour are also presented. Similar to Vatankhahghadim and Damaren (2019), the coupled deployment and stability dynamics problem in this paper is assumed to involve small enough displacements, compared to the system's large overall size, that a linearized study is justified. The reader is referred to Behdinan and Tabarrok (1997), Koivurova and Pramila (1997), Liu et al. (2014) for nonlinear dynamics of continua and solar sails, and to Zhang and Zu (1999), Öz et al. (2001), Wu et al. (2017) for examples of works that involve nonlinear stability analyses. In addition, similar to Vatankhahghadim and Damaren (2019) and many other works on translating continua, only ideal deployment is treated in this manuscript, assuming complete boom-membrane attachment (with no imperfections) and equal deployment rates on all booms. Treating such non-idealities and their influence on the solar sail system's dynamics and stability offer interesting paths for future work.

Upon validating the constant-length results against those in Hassanpour and Damaren (2018) via modal analysis, dynamic simulations are performed using a constant-rate deployment profile. In contrast to the energy-based approach of Vatankhahghadim and Damaren (2019) that yielded analytic expressions for assessing boundedness of vibration energy (a measure of dynamic stability), the present work adopts the kinetic vibration approach that yields a quadratic eigenvalue problem. Numerical eigenvalue studies are then performed, and the results seem to suggest the existence of instability regions in terms of amplitude growth — an aspect not accounted for by the energy-only approach of Vatankhahghadim and Damaren (2019) — for certain combinations of extension rate and sail tension.

The organization of this document is as follows: Section 2 describes the model of interest and some simplifying assumptions to make the problem tractable. The discretization approach of and the quadrant equations of motion from Vatankhahghadim and Damaren (2019) are reviewed in Section 3 and Appendix A, and more details are provided on extending these derivations to a complete sail. Also presented in Section 3 is a reformulation of the problem to enable numerical stability analyses. Simulation results pertinent to constant-length and deploying sails are presented in Section 4, along with those on the sail's deployment stability.

2. Model description and assumptions

A square solar sail model as shown in Fig. 1 is considered. Only out-of-plane deflections of the sail quadrants and their support booms are considered in the present document, and accounting for the in-plane deflections and the possibility of wrinkling are left as part of future work. Uniform thin membranes with no bending stiffness and Euler-Bernoulli beams with no axial extensibility are used to

Please cite this article as: B. Vatankhahghadim and C. J. Damaren, Solar sail deployment dynamics, Advances in Space Research, https://doi.org/10.1016/j.asr.2020.03.029

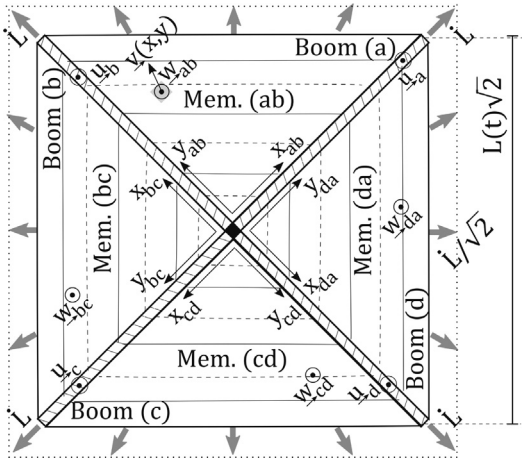

Fig. 1. Model of Deploying Solar Sail: Booms (a), (b), (c), and (d); and Membranes (ab), (bc), (cd), (da) with Straight Free Edges.

model the sail and the booms, respectively. Consistent with Vatankhahghadim and Damaren (2019), a sliding-type deployment is assumed, with the free edge remaining straight and at 45° to the booms at all times. This assumption is admittedly unrealistic, especially considering the many folds to which packaged sails are subjected, but it is a key assumption to render the problem tractable, and is believed to capture the main behaviour of the system upon which future higher fidelity studies can build. The resulting velocity distribution is presented in Vatankhahghadim and Damaren (2019) and Appendix A.

The membrane quadrants are taken to be under linearly increasing (towards the boom tips) forces per unit length, namely normal N_{xx} and N_{yy} and shear N_{xy}, provided by the booms. This results in compressive axial loads, P, on the latter. The corresponding expressions related to Membrane (ab) and Boom (a), for example, are Vatankhahghadim and Damaren (2019):

$$N_{xx} = N_{yy} = -N_{xy} = \frac{\bar{\sigma} h}{L_0}(x_{ab} + y_{ab}), \quad P_a = -\frac{\bar{\sigma} A}{L_0} x_{ab} \tag{1}$$

where $\bar{\sigma}$ is the initial maximum prestress near the boom tips, h is the uniform membrane thickness, and A and $L(t)$ are the booms' uniform cross-sectional area and time-varying length, respectively, with $L_0 = L(0)$. As further detailed in Vatankhahghadim and Damaren (2019), the force terms in Eq. (1) affect the strain energy used in the Lagrangian formulation, hence appearing in the stiffness matrices presented in Eqs. (A.1d) and (A.2d) in Appendix A. In the absence of wrinkling, future work that will also account for the in-plane deflections can use a linear Hookean constitutive relation to obtain the stress from the strains and deflections.

3. Discretized equations of motion

The quasi-modal approach with time-varying basis functions used by Cloutier (1968), Weeks (1986), Wang and Wei (1987), Janković (1979), Wang et al. (2009) is adopted. Focusing on Quadrant (ab) as an example, the out-of-plane deflections of the booms and the membrane — superimposed over the booms' deflections as in Shaker (1976), for constant length, and in Weeks (1986), for deployment — are expanded, using n_B and n_M modes, respectively, as Vatankhahghadim and Damaren (2019):

$$u_a(x_{ab},t) = \boldsymbol{p}_a^\intercal(t)\boldsymbol{\Psi}_a(x_{ab},t), \quad u_b(y_{ab},t) = \boldsymbol{p}_b^\intercal(t)\boldsymbol{\Psi}_b(y_{ab},t) \tag{2a}$$

$$w_{ab}(x_{ab},y_{ab},t) = u_a(x_{ab},t) + u_b(y_{ab},t) + \boldsymbol{q}_{ab}^\intercal(t)\boldsymbol{\Phi}_{ab}(x_{ab},y_{ab},t) \tag{2b}$$

where $\boldsymbol{p}_a \in \mathbb{R}^{n_B}, \boldsymbol{p}_b \in \mathbb{R}^{n_B}$, and $\boldsymbol{q}_{ab} \in \mathbb{R}^{n_M}$ are the generalized coordinates of Boom (a), Boom (b) and Membrane (ab), respectively. The time-varying components of $\boldsymbol{\Psi}_a$, $\boldsymbol{\Psi}_b$, and $\boldsymbol{\Phi}_{ab}$, which are the eigenfunctions of a cantilevered beam and an all-edges clamped membrane, depend on $x/L(t)$ and/or $y/L(t)$. It should be noted that one of the sources of error in the numerical results is the truncation of the series in Eq. (2), which are supposed to converge to accurate values only as $n \to \infty$.

3.1. Quadrant-level equations of motion

Using the expansions in Eq. (2) and the standard Lagrangian mechanics-based formulation involving the components' kinetic and strain potential energy expressions, the following discretized equations of motion (with the matrices in Appendix A) were obtained in Vatankhahghadim and Damaren (2019) for a single quadrant consisting of Membrane (ab) attached to Booms (a) and (b):

$$\begin{aligned}\left[\tilde{\boldsymbol{M}}_M + \tilde{\boldsymbol{M}}_B\right]\ddot{\tilde{\boldsymbol{q}}} + \left[\left(\dot{\tilde{\boldsymbol{M}}}_M + \dot{\tilde{\boldsymbol{M}}}_B\right) + \left(\tilde{\boldsymbol{G}}_M - \tilde{\boldsymbol{G}}_M^\intercal\right)\right. \\ \left. + \left(\tilde{\boldsymbol{G}}_B - \tilde{\boldsymbol{G}}_B^\intercal\right)\right]\dot{\tilde{\boldsymbol{q}}} + \left[\left(\dot{\tilde{\boldsymbol{G}}}_M + \dot{\tilde{\boldsymbol{G}}}_B\right) + \left(\Delta\tilde{\boldsymbol{K}}_M + \Delta\tilde{\boldsymbol{K}}_B\right)\right]\tilde{\boldsymbol{q}} = \boldsymbol{0}\end{aligned} \tag{3}$$

where $\tilde{\boldsymbol{q}} \triangleq \left[\boldsymbol{p}_a^\intercal \ \boldsymbol{p}_b^\intercal \ \boldsymbol{q}_{ab}^\intercal\right]^\intercal$ contains all of Quadrant (ab)'s generalized coordinates, and $\Delta\tilde{\boldsymbol{K}}_M \triangleq \boldsymbol{K}_{M,U} - \boldsymbol{K}_{M,T}$ and $\Delta\tilde{\boldsymbol{K}}_B \triangleq \boldsymbol{K}_{B,U} - \boldsymbol{K}_{B,T}$. The quadrant-level matrices denoted by a tilde are of dimensions $\tilde{n} \times \tilde{n}$ with $\tilde{n} = 2n_B + n_M$, and are constructed via spatial integration of some functions of $\boldsymbol{\Psi}$ and $\boldsymbol{\Phi}$, as provided in Appendix A. Note that the boom-related matrices (with the subscript 'B') have zero partitions corresponding to the membrane's generalized coordinates: for example, $\tilde{\boldsymbol{M}}_B \triangleq \text{blockdiag}\{\boldsymbol{M}_B, \boldsymbol{M}_B, \boldsymbol{0}_{n_M \times n_M}\}$, where the inner blocks (without a tilde) are those in Appendix A.

The square bracketed terms could be loosely viewed from left to right as effective mass, gyricity, and stiffness matrices. If a model of the system's structural damping is also available, it can be added to the second set of matrices, but it is believed that as long as the dissipative effects are sufficiently small compared to the gyroscopic forces, the stability results would be conservative and can benefit from small damping. For example, it was shown in Stylianou

Please cite this article as: B. Vatankhahghadim and C. J. Damaren, Solar sail deployment dynamics, Advances in Space Research, https://doi.org/10.1016/j.asr.2020.03.029

and Tabarrok (1994) that the onset of divergence instability of an extruding beam is not affected by physical damping, while its flutter instability is postponed. Caution must be taken, however, that there is possibility of destabilizing effects from damping in some gyroscopic systems (Ziegler, 1956; Nemat-Nasser et al., 1966).

3.2. System-level equations of motion

Recognizing a need for completeness in modelling and simulation, the present work first provides more details on how the formulation of Section 3.1 can be extended to apply to a complete four-quadrant sail. To achieve this extension, the quadrant-level matrices are "lifted" into system-level forms that correspond to the system-level collection of *all* generalized coordinates, $\bar{\mathbb{q}} \triangleq \begin{bmatrix} \boldsymbol{p}_a^\intercal & \boldsymbol{p}_b^\intercal & \boldsymbol{p}_c^\intercal & \boldsymbol{p}_d^\intercal & \boldsymbol{q}_{ab}^\intercal & \boldsymbol{q}_{bc}^\intercal & \boldsymbol{q}_{cd}^\intercal & \boldsymbol{q}_{da}^\intercal \end{bmatrix}^\intercal$. First, each of the quadrant-level matrices are partitioned into nine submatrices (for example $\tilde{\boldsymbol{M}}_{\mathrm{M,ab},ij}$ with $i,j \in \{1,2,3\}$) that correspond to $\boldsymbol{p}_a, \boldsymbol{p}_b$, and $\boldsymbol{q}_{ab}$, as follows:

$$\tilde{\boldsymbol{M}}_{\mathrm{M,ab}} = \left[\begin{array}{c:c:c} \overset{n_B}{\tilde{\boldsymbol{M}}_{\mathrm{M,ab},11}} & \overset{n_B}{\tilde{\boldsymbol{M}}_{\mathrm{M,ab},12}} & \overset{n_M}{\tilde{\boldsymbol{M}}_{\mathrm{M,ab},13}} \\ \hdashline \tilde{\boldsymbol{M}}_{\mathrm{M,ab},21} & \tilde{\boldsymbol{M}}_{\mathrm{M,ab},22} & \tilde{\boldsymbol{M}}_{\mathrm{M,ab},23} \\ \hdashline \tilde{\boldsymbol{M}}_{\mathrm{M,ab},31} & \tilde{\boldsymbol{M}}_{\mathrm{M,ab},32} & \tilde{\boldsymbol{M}}_{\mathrm{M,ab},33} \end{array}\right] \begin{array}{l} n_B \\ n_B \\ n_M \end{array} \tag{4}$$

The system-level mass matrix corresponding to Quadrant (ab)'s membrane, denoted by $\bar{\mathbb{M}}_{\mathrm{M,ab}}$ and of dimensions $\bar{n} \times \bar{n}$ with $\bar{n} = 4n_B + 4n_M$, can be partitioned into 64 blocks, namely $\bar{\mathbb{M}}_{\mathrm{M,ab},pq}$ with $p,q \in \{1,\cdots,8\}$. Of these 64 blocks, nine are replaced by $\tilde{\boldsymbol{M}}_{\mathrm{M,ab},ij}$ in Eq. (4), and the rest are all zero matrices of appropriate dimensions. Summarized in Table 1 is the mapping between the indices of the quadrant-level and system-level matrices. For example, the $\tilde{\boldsymbol{M}}_{\mathrm{M,ab},23}$ block of the quadrant-level $\tilde{\boldsymbol{M}}_{\mathrm{M,ab}}$ replaces the $\bar{\mathbb{M}}_{\mathrm{M,ab},25}$ block of the system-level $\bar{\mathbb{M}}_{\mathrm{M,ab}}$, because the generalized coordinates of Boom (b) and Quadrant (ab), the second and third blocks of $\tilde{q}$, are now in the second and fifth blocks of $\bar{\mathbb{q}}$.

Lastly, after all matrices in Eq. (3) for all quadrants are lifted into their system-level form using the above procedure and Table 1, the overall system matrices are computed by addition. For example, the membranes' total mass matrix is $\bar{\mathbb{M}}_{\mathrm{M}} = \bar{\mathbb{M}}_{\mathrm{M,ab}} + \bar{\mathbb{M}}_{\mathrm{M,bc}} + \bar{\mathbb{M}}_{\mathrm{M,cd}} + \bar{\mathbb{M}}_{\mathrm{M,da}}$. The resulting system matrices, replacing their quadrant-level counterparts in Eq. (3), along with the system-level coordinates in $\bar{\mathbb{q}}$ and their rates, describe the complete system's out-of-plane dynamics:

$$\underbrace{\left[\bar{\mathbb{M}}_{\mathrm{M}} + \bar{\mathbb{M}}_{\mathrm{B}}\right]}_{\bar{\mathbb{M}}_{\mathrm{eq}}} \ddot{\bar{\mathbb{q}}} + \underbrace{\left[\left(\dot{\bar{\mathbb{M}}}_{\mathrm{M}} + \dot{\bar{\mathbb{M}}}_{\mathrm{B}}\right) + \left(\bar{\mathbb{G}}_{\mathrm{M}} - \bar{\mathbb{G}}_{\mathrm{M}}^\intercal\right) + \left(\bar{\mathbb{G}}_{\mathrm{B}} - \bar{\mathbb{G}}_{\mathrm{B}}^\intercal\right)\right]}_{\bar{\mathbb{G}}_{\mathrm{eq}}} \dot{\bar{\mathbb{q}}} + \underbrace{\left[\left(\dot{\bar{\mathbb{G}}}_{\mathrm{M}} + \dot{\bar{\mathbb{G}}}_{\mathrm{B}}\right) + \left(\Delta\bar{\mathbb{K}}_{\mathrm{M}} + \Delta\bar{\mathbb{K}}_{\mathrm{B}}\right)\right]}_{\bar{\mathbb{K}}_{\mathrm{eq}}} \bar{\mathbb{q}} = \boldsymbol{0} \tag{5}$$

where $\Delta\bar{\mathbb{K}}_{\mathrm{M}} \triangleq \bar{\mathbb{K}}_{\mathrm{M,U}} - \bar{\mathbb{K}}_{\mathrm{M,T}}$ and $\Delta\bar{\mathbb{K}}_{\mathrm{B}} \triangleq \bar{\mathbb{K}}_{\mathrm{B,U}} - \bar{\mathbb{K}}_{\mathrm{B,T}}$. For simplicity, new system-level matrices $\bar{\mathbb{M}}_{\mathrm{eq}}$, $\bar{\mathbb{G}}_{\mathrm{eq}}$, and $\bar{\mathbb{K}}_{\mathrm{eq}}$ are defined to denote the "equivalent" mass, gyricity, and stiffness matrices. However, they do not possess the same symmetry and definiteness properties typically associated with these terms. For example, $\bar{\mathbb{K}}_{\mathrm{eq}}$ is not necessarily positive-definite.

3.3. Quadratic eigenvalue problem

The kinetic vibration approach (so-termed in Ziegler (1977)) to stability is adopted in this work. Upon assuming solutions of exponential form, the system in Eq. (5) leads to the following quadratic eigenvalue problem:

$$\bar{\mathbb{M}}_{\mathrm{eq}}\ddot{\bar{\mathbb{q}}} + \bar{\mathbb{G}}_{\mathrm{eq}}\dot{\bar{\mathbb{q}}} + \bar{\mathbb{K}}_{\mathrm{eq}}\bar{\mathbb{q}} = \boldsymbol{0} \;\Rightarrow\; \det\left(\lambda^2\bar{\mathbb{M}}_{\mathrm{eq}} + \lambda\bar{\mathbb{G}}_{\mathrm{eq}} + \bar{\mathbb{K}}_{\mathrm{eq}}\right) = 0 \tag{6}$$

which leads to $2\bar{n} = 8n_B + 8n_M$ eigenvalues. Problems of this type were considered in detail in Tisseur and Meerbergen (2001), and algorithms (claimed to be superior for certain problems) are available, for example in Hammarling et al. (2013), that attempt to solve them by avoiding a reformulation into a first-order form. However, similar to Niemi and Pramila (1987), Shin et al. (2005), the following form that allows consistent determination and sorting of the eigenvalues (via *eigenshuffle( )* in MATLAB) is used, assuming invertibility of $\bar{\mathbb{M}}_{\mathrm{eq}}$:

$$\dot{\bar{\mathbb{x}}} = \underbrace{\begin{bmatrix} -\bar{\mathbb{M}}_{\mathrm{eq}}^{-1}\bar{\mathbb{G}}_{\mathrm{eq}} & -\bar{\mathbb{M}}_{\mathrm{eq}}^{-1}\bar{\mathbb{K}}_{\mathrm{eq}} \\ 1 & \boldsymbol{0} \end{bmatrix}}_{\bar{\mathbb{C}}} \bar{\mathbb{x}} \;\Rightarrow\; \det\left(\lambda 1 - \bar{\mathbb{C}}\right) = 0 \tag{7}$$

where $\dot{\bar{\mathbb{x}}} \triangleq \begin{bmatrix} \dot{\bar{\mathbb{q}}}^\intercal & \bar{\mathbb{q}}^\intercal \end{bmatrix}^\intercal$ it is worth emphasizing that, despite having formulated an eigenvalue problem for the system of interest, the matrices associated with a given deployment scenario are time-varying and they do not, in general, offer clear implications about stability. In other words, the eigenvalues are not "natural frequencies" of the system owing to its time-varying nature. In terms of past works on stability analysis, the parameter variations in Stylianou and Tabarrok (1994), for example, were interpreted in two ways (Stylianou, 1993): keeping the boom length fixed and varying the rate, treating each simulation case as an independent deployment scenario; and vice versa, changing length over time during a given deploy-

Table 1
Mapping between Block Indices of the Partitioned Quadrant-Level and System-Level Matrices.

Quadrant	(ab)			(bc)			(cd)			(da)		
Quadrant-Level (i,j)	1	2	3	1	2	3	1	2	3	1	2	3
System-Level (p,q)	1	2	5	2	3	6	3	4	7	4	1	8

Please cite this article as: B. Vatankhahghadim and C. J. Damaren, Solar sail deployment dynamics, Advances in Space Research, https://doi.org/10.1016/j.asr.2020.03.029

ment scenario. It is the former interpretation that is adopted here, and was also used in Wang et al. (2010) to study the stability of deploying plates of varying length, for it is more meaningful, but the resulting critical values would be the same with both viewpoints (Stylianou, 1993).

4. Results and discussion

Numerical simulations are performed using some of the solar sail parameters considered in Choi (2015), unless otherwise stated, including $\rho = 4.64 \times 10^{-2}$ kg/m, $EI = 4.62 \times 10^{3}$ N · m^2, and $A = 3.22 \times 10^{-5}$ m^2 for all of the booms; and $\mu = 1.39 \times 10^{-2}$ kg/m^2 (or $\mu = 1.39 \times 10^{-1}$ kg/m^2 for heavier membranes) and $h = 1 \times 10^{-5}$ m for all of the membrane quadrants. The constant-length and deploying sail simulations of Sections 4.1 and 4.2 are based on Eq. (5), while the stability results in Section 4.3 are obtained using Eq. (7). All dynamic simulations use the Newmark-Beta algorithm of Newmark (1959) with $\beta = 1/2$ and a step-size of 10^{-4} s. The numbers of modes used for each boom and membrane in the expansions described in Section 3 are set to $n_B = 4$ and $n_M = 16$, respectively. A plausible explanation of the stability results is offered in Section 4.4.

4.1. Validation

Before studying deployment, validation of the basics of the modelling and simulation using past literature is in order. To this end, the mode shapes and frequencies of the entire sail, after full deployment into a 100 m × 100 m square shape with a pretension profile given by $\bar{\sigma} = 100$ kPa, are compared against those obtained in Hassanpour and Damaren (2018) using a different FEM-based formulation. The first 6 modal frequencies, obtained upon neglecting axial tension imposed on the booms in Eq. (1) — consistent with Hassanpour and Damaren (2018) — and using the same parameters, in turn based on those in Choi (2015), are listed in Table 2. They show less than 3% discrepancy compared to those reported in Hassanpour and Damaren (2018), and the associated mode shapes presented in Fig. 2 resemble those in Hassanpour and Damaren (2018). As expected, the complete sail has additional symmetric/anti-symmetric modes that would not appear in the single sail quadrant that was the primary focus of Vatankhahghadim and Damaren (2019).

4.2. Deployment simulation

To focus on how deflections propagate from a single corner on the sail to other areas, the results shown in Fig. 3 have only their Boom (a) — along the positive and negative x-axis — initially deflected by −0.2 m via $\boldsymbol{p}_a(0) = [1\ 0\ 0\ 0]^T/L(0)$ and $\dot{\boldsymbol{p}}_a(0) = \boldsymbol{0}_{4\times1}$, and the rest of the initial conditions are set to zero. Both sets of results use a smaller tension (compared to Section 4.1) of $\bar{\sigma} = 2$ kPa, now with the booms' compression in Eq. (1) also modelled, but they differ from each other in terms of their membrane mass: the sail in Fig. 3i has a membrane mass density of $\mu = 1.39 \times 10^{-2}$ kg/m^2, but the sail in Fig. 3ii uses a heavier sail membrane with

Table 2
Comparison of the First 6 Modal Frequencies (for Fully Deployed Sail) Using the Present Approach vs. FEM in Hassanpour and Damaren (2018).

Modal Frequency	ω_1	ω_2	ω_3	ω_4	ω_5	ω_6
Using FEM (rad/s)	0.05180	0.20848	0.20848	0.30520	0.36781	0.36781
Present Method (rad/s)	0.05328	0.20954	0.20954	0.31002	0.37091	0.37091

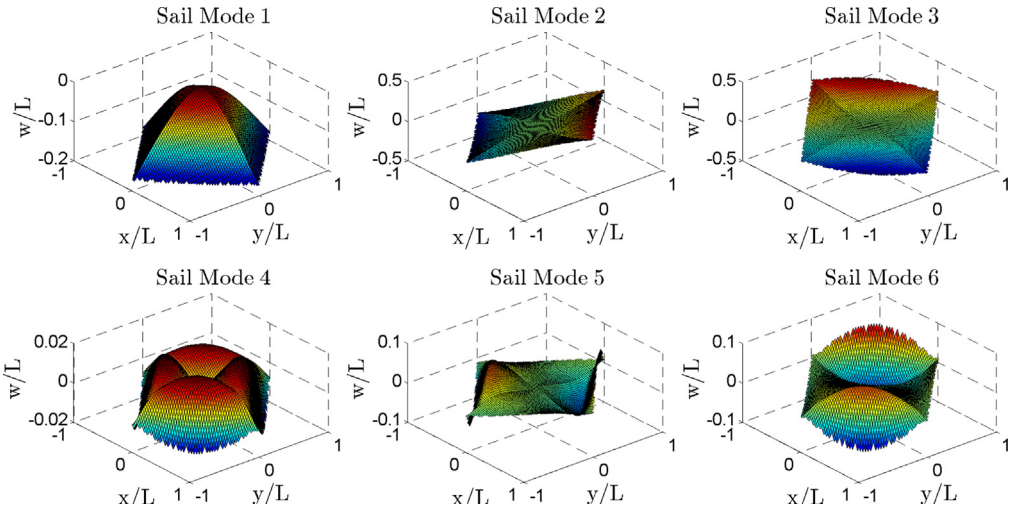

Fig. 2. First 6 Modes of Solar Sail with Boom Length $L = 50\sqrt{2}$ m (for Comparison against Fig. 6 in Hassanpour and Damaren (2018)).

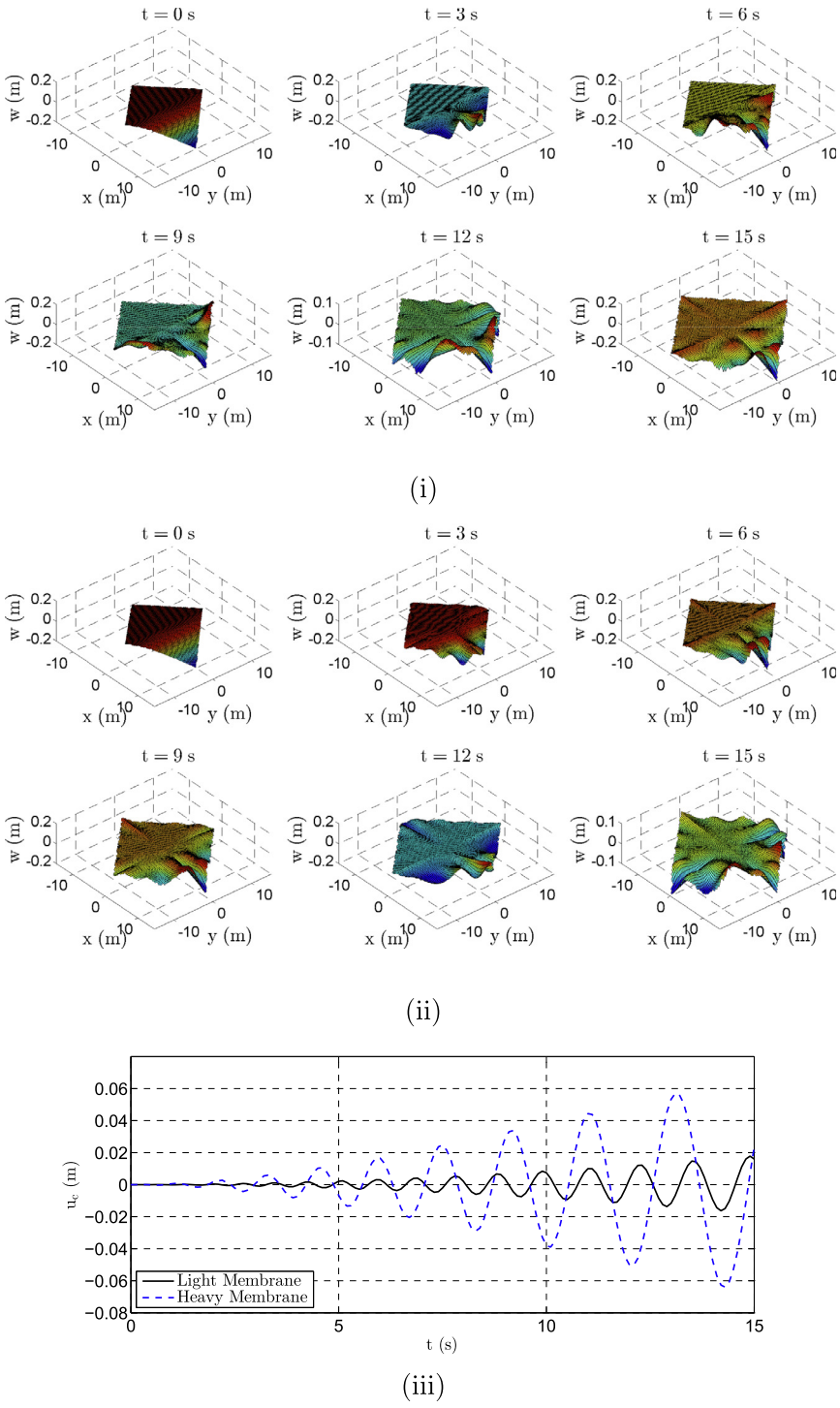

Fig. 3. Simulated Constant-Rate Sail Deployment with Asymmetric ICs (from $L(0) = 10$ m to $L(t_f) = 15$ m in 15 s): (i) Light Membrane with $\mu = 1.39 \times 10^{-2}$ kg/m^2, (ii) Heavy Membrane with $\mu = 1.39 \times 10^{-1}$ kg/m^2, and (iii) Comparison of Boom (c) Tip Deflection Histories in Both Sails.

$\mu = 1.39 \times 10^{-1}$ kg/m^2. The booms' length profile is given by $L(t) = 10 + (1/3)t$. The aim is to assess the relative effect of membrane quadrants on the booms, and to help facilitate this, provided in Fig. 3iii are the tip deflections of Boom (c), along negative x-axis and at the furthest corner from the point of initial displacement. The results, showing larger deflections in Fig. 3ii than in Fig. 3i, suggest the presence of a heavier membrane entails more pronounced propagation of deflections throughout the sail.

4.3. Stability results

The effects of each parameter of interest, namely deployment rate and pretension, are studied as described in Sec-

Please cite this article as: B. Vatankhahghadim and C. J. Damaren, Solar sail deployment dynamics, Advances in Space Research, https://doi.org/10.1016/j.asr.2020.03.029

tion 3.3, upon fixing the boom length and performing a "frozen" eigenvalue analysis. Given that an eigenvalue with a positive real part implies instability, the resulting eigenvalues are sorted in descending order based on their real parts. Shown in Fig. 4 are the changes in the real and imaginary parts of the first 3 distinct eigenvalues as the tip tension, $\bar{\sigma}$, is varied, while the deployment rate is assumed to be a constant value. Since some modes are equivalent because of the system's symmetry, resulting in each set of 4 modes having the same eigenvalue, the distinct ones correspond to the first, fourth, and ninth eigenvalues. Each of the three parts (i), (ii), and (iii) of Fig. 4 corresponds to a different value of extension rate, $\dot{L}$, namely 0.3, 0.5, and 0.7 m/s, respectively. Owing to the fact that a frozen study is being conducted using specific values of boom length, the results are produced using different values

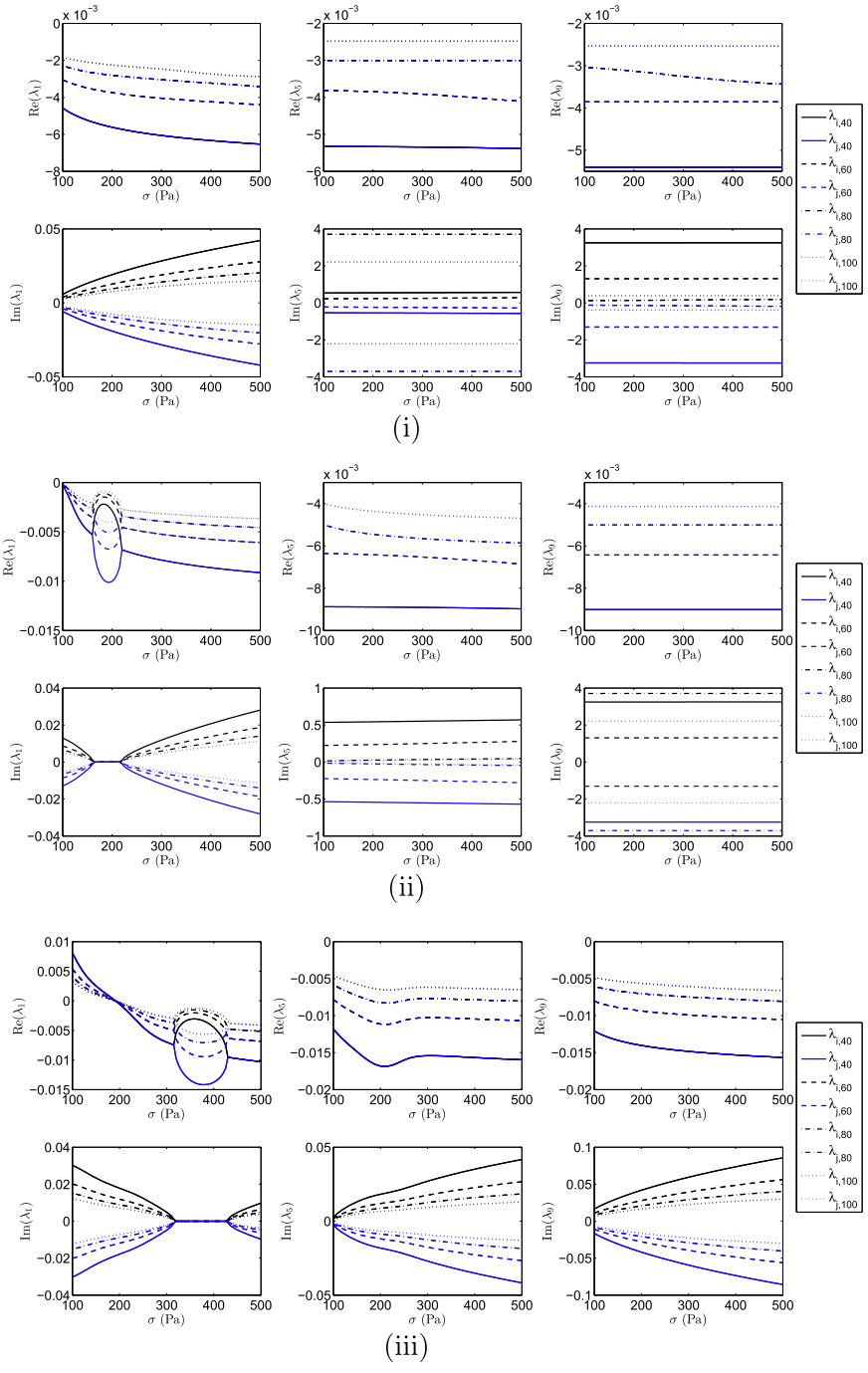

Fig. 4. Light Membrane ($\mu = 1.39 \times 10^{-2}$ kg/m^2) - Real (Upper) and Imaginary (Lower) Parts of Pairs (Blue and Black) of Eigenvalues Corresponding to First 3 Distinct Modes vs. Pretension Magnitude, Using Various Lengths (Different Line Patterns) and Various Extension Rates: (i) $\dot{L} = 0.3$ m/s, (ii) $\dot{L} = 0.5$ m/s, and (iii) $\dot{L} = 0.7$ m/s. (For interpretation of the references to colour in this figure legend, the reader is referred to the web version of this article.)

Please cite this article as: B. Vatankhahghadim and C. J. Damaren, Solar sail deployment dynamics, Advances in Space Research, https://doi.org/10.1016/j.asr.2020.03.029

of L, namely 40, 60, 80, and 100 m (shown with solid, dashed, dash-dotted, and dotted lines, respectively). The length corresponding to each pattern is indicated using a subscript in the relevant legend item: for example, $\lambda_{i,40}$ and $\lambda_{j,40}$ for a sail of boom length $L = 40$ m, where the subscripts i and j further distinguish between each part of the complex conjugate pairs associated with each eigenvalue.

The results show interesting effects caused by changes in the sail's pretension and deployment rate. In part (ii) of Fig. 4, the first mode experiences vanishing of oscillation frequency. A similar effect was observed in Wickert and Mote (1990), Lin (1997) and Shin et al. (2005), where a critical value of travel rate was obtained at which the frequency becomes zero. However, unlike those works that involved fixed-length travelling continua and similar to Stylianou and Tabarrok (1994) and Wang et al. (2009) that examined extending continua of varying lengths, the vanishing of the imaginary components in Fig. 4 does not imply divergence instability, since the corresponding real parts are still negative. Within the confines of the range of $\bar{\sigma}$ considered in this section, namely 100 to 500 Pa, further increase in extension rate (as is done in parts (iii) of Fig. 4) is required to introduce the possibility of the system's divergence instability, which occurs when the maximum tension drops below $\bar{\sigma} \approx 191$ Pa with $\dot{L} = 0.7$ m/s.

4.4. Discussion

It is believed that the change in the system's stability properties caused by increasing extension rate and tension can be attributed to the conflicting effects of the change in the system's stiffness and the energy transfer mechanisms involved. Mathematically, the most likely cause of instability are the $\tilde{\boldsymbol{G}}$ matrices presented in Eqs. (A.1b) and (A.2b) in Appendix A. These are the terms that carry the effects of the centrifugal forces within the system, and their contribution increases until at some point, as mentioned in Stylianou and Tabarrok (1994), Lee and Mote (1997a) (for translating beams), they overcome the stabilizing effects of the flexural restoring forces, while the effect of the stiffness terms in the $\tilde{\boldsymbol{K}}$ matrices in Eqs. (A.1c) and (A.2c) in Appendix A diminishes.

The question then becomes: why do the results show instability only for low boundary stresses? As shown in Wickert and Mote (1989), Lee and Mote (1997a), Lee and Mote (1997b), Zhu (2002), the energy in translating strings and tensioned beams is not conserved, and the change in energy is explained by the energy flux through the boundaries and the work done by the non-conservative boundary forces on the system. It was further explained in Lee and Mote (1997a), Lee and Mote (1997a) that the tensile forces at a fixed boundary upstream of translating strings (second-order systems) produce negative energy flux, so do the Coriolis forces at a free boundary downstream of translating tensioned beams (fourth-order systems). Given that the rate of change of energy from a control volume viewpoint is directly related to dynamic stability (Zhu, 2002), it is reasonable to expect that decreasing tensile forces for a given deployment rate will have destabilizing effects: below a threshold, they no longer provide the negative flux needed to overcome the aforementioned destabilizing contribution of the growing $\tilde{\boldsymbol{G}}$ terms. One more observation with regards to Fig. 4 is that not all vibration modes experience divergence instability at the same time. This observation is also consistent with what was pointed out in some past works on axially translating continua, such as in Wickert and Mote (1988) where fourth-order beam-like systems' dispersive nature is recognized to be responsible for different critical speeds of each vibration mode.

5. Conclusions

Inspired by and building upon an extensive body of literature on the dynamics of translating continua, this paper presents dynamics and stability simulation results related to the deployment of a hybrid system of moving continua, namely a multibody system of flexible beams (mathematically second-order) and thin membranes (fourth-order). The presented formulation extends that of Vatankhahghadim and Damaren (2019) on a single quadrant, and its stability analysis complements the results of that work and sheds more light on the vibration characteristics of solar sails during deployment.

Assuming the discretized equations of motion for a single quadrant are known and upon providing the expressions for the associated matrices, this document details a "lifting" procedure on the matrices to enable their use in the extended system-level equations of motion. The resulting system of second-order differential equations is then recast into first-order form, and the kinetic (vibration) approach to stability is adopted by conducting an eigenvalue analysis on the resulting system. Numerical integration of the equations of motion and computation of the system's "frozen" (at a given length) eigenvalues are performed. The modelling and simulation results are validated by comparison against constant-length modal analysis via FEM from past literature. The stability analysis results show possibility of divergence if the membrane pretension is below a threshold, which increases as the extension rate increases. This phenomenon could be potentially attributed to the boundary tensile forces' negative energy flux.

Acknowledgement

This research was supported by the Ontario Graduate Scholarship (OGS) program, jointly funded by the Province of Ontario and the University of Toronto. Additional work to address the revisions was supported by the Natural Sciences and Engineering Research Council of Canada (NSERC).

Please cite this article as: B. Vatankhahghadim and C. J. Damaren, Solar sail deployment dynamics, Advances in Space Research, https://doi.org/10.1016/j.asr.2020.03.029

Appendix A. Quadrant-level matrices

To significantly improve computational efficiency, the problem in Vatankhahghadim and Damaren (2019) was transformed from that of spatially fixed points within time-varying boundaries, namely $x$and $y$that satisfy $0 < x < L(t)$ and $0 < y < L(t)$, to that of moving points within fixed boundaries, namely $\hat{x} \triangleq x/L(t)$ and $\hat{y} \triangleq y/L(t)$ that satisfy $0 < \hat{x}(t) < 1$ and $0 < \hat{y}(t) < 1$ (as was done in Bergamaschi and Sinopoli (1983), Hughes (1976), Behdinan and Tabarrok (1997), among others). With this transformation, the following boom-related matrices were obtained in Vatankhahghadim and Damaren (2019):

$$\boldsymbol{M}_{\mathrm{B}} = \rho L \int_{0^+}^{1} \boldsymbol{\Psi}_{\mathrm{a}} \boldsymbol{\Psi}_{\mathrm{a}}^{\mathsf{T}} \, d\hat{x} \tag{A.1a}$$

$$\boldsymbol{G}_{\mathrm{B}} = \rho \dot{L} \int_{0^+}^{1} (1-\hat{x}) \boldsymbol{\Psi}_{\mathrm{a}} \boldsymbol{\Psi}_{\mathrm{a},\hat{x}}^{\mathsf{T}} \, d\hat{x} \tag{A.1b}$$

$$\boldsymbol{K}_{\mathrm{B,T}} = \rho \frac{\dot{L}^2}{L} \int_{0^+}^{1} (1-\hat{x})^2 \boldsymbol{\Psi}_{\mathrm{a},\hat{x}} \boldsymbol{\Psi}_{\mathrm{a},\hat{x}}^{\mathsf{T}} \, d\hat{x} \tag{A.1c}$$

$$\boldsymbol{K}_{\mathrm{B,U}} = -\frac{\bar{\sigma} A}{L_0} \int_{0^+}^{1} \hat{x} \boldsymbol{\Psi}_{\mathrm{a},\hat{x}} \boldsymbol{\Psi}_{\mathrm{a},\hat{x}}^{\mathsf{T}} \, d\hat{x} + \frac{EI}{L^3} \int_{0^+}^{1} \boldsymbol{\Psi}_{\mathrm{a},\hat{x}\hat{x}} \boldsymbol{\Psi}_{\mathrm{a},\hat{x}\hat{x}}^{\mathsf{T}} \, d\hat{x} \tag{A.1d}$$

where ρ and EI are the booms' mass density per unit length and bending stiffness, respectively. The commas in the subscripts denote differentiation with respect to the variables that follow them. The column matrix $\boldsymbol{\Psi}_{\mathrm{a}}(\hat{x})$ stores the beam eigenfunctions in terms of $\hat{x}$, and $\boldsymbol{\Psi}_{\mathrm{a},\hat{x}}(\hat{x}) = L\boldsymbol{\Psi}_{\mathrm{a},x}$ and $\boldsymbol{\Psi}_{\mathrm{a},\hat{x}\hat{x}}(\hat{x}) = L^2\boldsymbol{\Psi}_{\mathrm{a},xx}$ are its spatial derivatives with respect to $\hat{x}$. Since all of the integrals of Eq. (A.1) are only $\hat{x}$-dependent, numerical integration is required only once, and not at each time-step. As another welcome consequence of the coordinate transformation, the rate matrices $\dot{\tilde{\boldsymbol{M}}}_B$ and $\dot{\tilde{\boldsymbol{G}}}_B$ are readily obtained by applying the chain rule to the coefficients outside the integrals. Note that the matrices in Eq. (A.1) are placed in quadrant-level augmented $n \times n$ block-diagonal form before their use in Eq. (3). For example, $\tilde{\boldsymbol{M}}_{\mathrm{B}} \triangleq \mathrm{blockdiag}\{\boldsymbol{M}_{\mathrm{B}}, \boldsymbol{M}_{\mathrm{B}}, \boldsymbol{0}_{n_{\mathrm{M}} \times n_{\mathrm{M}}}\}$.

Similarly, the following membrane-related matrices were obtained in Vatankhahghadim and Damaren (2019):

$$\tilde{\boldsymbol{M}}_{\mathrm{M}} = \mu L^2 \int_{0^+}^{1} \int_{0^+}^{1-\hat{x}} \hat{\tilde{\boldsymbol{A}}} \hat{\tilde{\boldsymbol{A}}}^{\mathsf{T}} \, d\hat{y} \, d\hat{x} \tag{A.2a}$$

$$\tilde{\boldsymbol{G}}_{\mathrm{M}} = \mu L \dot{L} \int_{0^+}^{1} \int_{0^+}^{1-\hat{x}} \hat{\tilde{\boldsymbol{A}}} \hat{\tilde{\boldsymbol{B}}}^{\mathsf{T}} \, d\hat{y} \, d\hat{x} \tag{A.2b}$$

$$\tilde{\boldsymbol{K}}_{\mathrm{M,T}} = \mu \dot{L}^2 \int_{0^+}^{1} \int_{0^+}^{1-\hat{x}} \hat{\tilde{\boldsymbol{B}}} \hat{\tilde{\boldsymbol{B}}}^{\mathsf{T}} \, d\hat{y} \, d\hat{x} \tag{A.2c}$$

$$\tilde{\boldsymbol{K}}_{\mathrm{M,U}} = \frac{\bar{\sigma} h L}{L_0} \int_{0^+}^{1} \int_{0^+}^{1-\hat{x}} (\hat{x}+\hat{y}) \Big(\hat{\tilde{\boldsymbol{C}}} \hat{\tilde{\boldsymbol{C}}}^{\mathsf{T}} + \hat{\tilde{\boldsymbol{D}}} \hat{\tilde{\boldsymbol{D}}}^{\mathsf{T}} - \Big(\hat{\tilde{\boldsymbol{C}}} \hat{\tilde{\boldsymbol{D}}}^{\mathsf{T}} + \hat{\tilde{\boldsymbol{D}}} \hat{\tilde{\boldsymbol{C}}}^{\mathsf{T}} \Big) \Big) \, d\hat{y} \, d\hat{x} \tag{A.2d}$$

where μ is the membrane's mass density per unit area, and the following intermediate matrices are used:

$$\hat{\tilde{\boldsymbol{A}}} \triangleq \begin{bmatrix} \boldsymbol{\Psi}_{\mathrm{a}} \\ \boldsymbol{\Psi}_{\mathrm{b}} \\ \boldsymbol{\Phi} \end{bmatrix}, \; \hat{\tilde{\boldsymbol{C}}} \triangleq \begin{bmatrix} \boldsymbol{\Psi}_{\mathrm{a},\hat{x}} \\ \boldsymbol{0} \\ \boldsymbol{\Phi}_{,\hat{x}} \end{bmatrix}, \; \hat{\tilde{\boldsymbol{D}}} \triangleq \begin{bmatrix} \boldsymbol{0} \\ \boldsymbol{\Psi}_{\mathrm{b},\hat{y}} \\ \boldsymbol{\Phi}_{,\hat{y}} \end{bmatrix},$$

$$\hat{\tilde{\boldsymbol{B}}} \triangleq (\hat{v}_{\hat{\mathrm{x}}} - \hat{x}) \hat{\tilde{\boldsymbol{C}}} + (\hat{v}_{\hat{\mathrm{y}}} - \hat{y}) \hat{\tilde{\boldsymbol{D}}}$$

where $\hat{\tilde{\boldsymbol{C}}}$ and $\hat{\tilde{\boldsymbol{D}}}$ contain derivatives of the eigenfunctions with respect to $\hat{x}$ and $\hat{y}$, necessitating the use of $1/L$ or $1/L^2$ factors for first and second derivatives. In addition, $\hat{v}_{\hat{\mathrm{x}}} = v_{\mathrm{x}}/\dot{L}$ and $\hat{v}_{\hat{\mathrm{y}}} = v_{\mathrm{y}}/\dot{L}$ where $v_{\mathrm{x}} = \dot{L}/2[1 + (x-y)/(x+y)]$ and $v_{\mathrm{y}} = \dot{L}/2[1 - (x-y)/(x+y)]$ are the x- and y-components of deployment velocity at (x, y) (Vatankhahghadim and Damaren, 2019). The same comments as those made about the boom matrices regarding computational efficiency hold.

References

Behdinan, K., Tabarrok, B., 1997. Dynamics of flexible sliding beams—non-linear analysis part II: transient response. J. Sound Vib. 208 (4), 541–565. https://doi.org/10.1006/jsvi.1997.1168.

Bergamaschi, S., Sinopoli, A., 1983. On the flexural vibrations of arms with variable length. An exact solution. Mech. Res. Commun. 10 (6), 341–344.

Block, J., Strauble, M., Wiedemann, M., 2011. Ultralight deployable booms for solar sails and other large gossamer structures in space. Acta Astronaut. 68 (7–8), 984–992.

Carrier, G.F., 1949. The spaghetti problem. Am. Math. Month. 56 (10), 669–672. https://doi.org/10.2307/2305560.

Cherchas, D.B., 1971. Dynamics of spin-stabilized satellites during extension of long flexible booms. J. Spacecraft Rockets 8 (7), 802–804. https://doi.org/10.2514/3.30323.

Cherchas, P.C., Gossain, D.M., 1974. Dynamics of a flexible solar array during deployment from a spinning spacecraft. C.A.S.I. Trans. 7 (1), 10–18.

Choi, M., 2015. Flexible Dynamics and Attitude Control of a Square Solar Sail (Ph.D. thesis). University of Toronto, Toronto, ON.

Cloutier, G.J., 1968. Dynamics of deployment of extendible booms from spinning space vehicles. J. Spacecraft Rockets 5 (5), 547–552. https://doi.org/10.2514/3.29303.

Hammarling, S., Munro, C.J., Tisseur, F., 2013. An algorithm for the complete solution of quadratic eigenvalue problems. ACM Trans. Math. Softw. 39 (3), 18:1–18:19. https://doi.org/10.1145/2450153.2450156.

Hassanpour, S., Damaren, C.J., 2018. Linear structural dynamics and modal cost analysis for a solar sail. In: AIAA Spacecraft Structures Conference, AIAA SciTech Forum. Kissimmee, FL., AIAA 2018-1434, https://doi.org/10.2514/6.2018-1434.

Hedgepeth, J.M., 1970. Dynamics of a large spin-stiffened deployable paraboloidal antenna. J. Spacecraft Rockets 7 (9), 1043–1048. https://doi.org/10.2514/3.30100.

Hughes, P.C., 1972. Dynamics of a spin-stabilized satellite during extension of rigid booms. C.A.S.I. Trans. 5 (1), 11–14.

Hughes, P.C., 1976. Deployment dynamics of the Communications Technology Satellite - a progress report. In: Proceedings of the ESRO Symposium on Dynamics and Control of Non-Rigid Spacecraft, vol. SP 117. Frascati, Italy, pp. 335–340.

Hughes, P.C., Garg, S.C., 1973. Dynamics of large flexible solar arrays and application to spacecraft attitude control system design. Tech.

Rep. 179. University of Toronto Institute for Aerospace Studies, Toronto, ON.

Janković, M.S., 1979. Deployment Dynamics of Flexible Spacecraft (Ph. D. thesis). University of Toronto, Toronto, ON.

Koivurova, H., Pramila, A., 1997. Nonlinear vibration of axially moving membrane by finite element method. Comput. Mech. 20 (6), 573–581. https://doi.org/10.1007/s004660050.

Lee, S.-Y.-., Mote Jr., C.D., 1997a. A generalized treatment of the energetics of translating continua, part I: strings and second order tensioned pipes. J. Sound Vib. 204 (5), 717–734. https://doi.org/10.1006/jsvi.1996.0945.

Lee, S.-Y.-., Mote Jr., C.D., 1997b. A generalized treatment of the energetics of translating continua, part II: beams and fluid conveying pipes. J. Sound Vib. 204 (5), 735–753. https://doi.org/10.1006/jsvi.1996.0946.

Leech, C.M., 1970. The Dynamics of Beams Under the Influence of Convecting Inertial Forces (Ph.D. thesis). University of Toronto, Toronto, ON.

Lin, C.C., 1997. Stability and vibration characteristics of axially moving plates. Int. J. Solids Struct. 34 (24), 3179–3190. https://doi.org/10.1016/S0020-7683(96)00181-3.

Liu, J., Cui, N., Shen, F., Rong, S., 2014. Dynamics of highly-flexible solar sail subjected to various forces. Acta Astronaut. 103, 55–72. https://doi.org/10.1016/j.actaastro.2014.06.030.

Miranker, W.L., 1960. The wave equation in a medium in motion. IBM J. Res. Dev. 4 (1), 36–42. https://doi.org/10.1147/rd.41.0036.

Mote Jr., C.D., 1972. Dynamic stability of axially moving materials. Shock Vib. Digest 4 (4), 2–11.

Nemat-Nasser, S., Prasad, S.N., Herrmann, G., 1966. Destabilizing effect of velocity-dependent forces in nonconservative continuous systems. AIAA J. 4 (7), 1276–1280. https://doi.org/10.2514/3.3659.

Newmark, N.M., 1959. A method of computation for structural dynamics. ASCE J. Eng. Mech. Div. 85 (3), 67–94.

Niemi, J., Pramila, A., 1987. FEM-analysis of transverse vibrations of an axially moving membrane immersed in ideal fluid. Int. J. Numer. Meth. Eng. 24 (12), 2301–2313. https://doi.org/10.1002/nme.1620241205.

Öz, H.R., Pakdemirli, M., Boyacı, H., 2001. Non-linear vibrations and stability of an axially moving beam with time-dependent velocity. Int. J. Non-Linear Mech. 36 (1), 107–115. https://doi.org/10.1016/S0020-7462(99)00090-6.

Pappa, R.S., Jones, T.W., Lunsford, C.B., Meyer, C.G., 2006. In-vacuum photogrammetry of a ten-meter square solar sail. Exp. Tech. 30 (3), 46–51. https://doi.org/10.1111/j.1747-1567.2006.00042.x.

Sack, R.A., 1954. Transverse oscillations in travelling strings. Br. J. Appl. Phys. 5 (6), 224–226. https://doi.org/10.1088/0508-3443/5/6/307.

Sakamoto, H., Miyazaki, y., Mori, O., 2011. Transient dynamic analysis of gossamer-appendage deployment using nonlinear finite element method. J. Spacecraft Rockets 48 (5), 881–890. https://doi.org/10.2514/1.52552.

Shaker, F.J., 1976. Free-vibration characteristics of a large split-blanket solar array in a 1-g field. Tech. Rep. TN D83–7576. NASA, Washington, D.C.

Shin, C., Chung, J., Kim, W., 2005. Dynamic characteristics of the out-of-plane vibration for an axially moving membrane. J. Sound Vib. 286 (4–5), 1019–1031. https://doi.org/10.1016/j.jsv.2005.01.013.

Shirasawa, Y., Mori, O., Miyazaki, Y., Sakamoto, H., Hasome, M., Okuizumi, N., Sawada, H., Furuya, H., Matsunaga, S., Natori, M., Kawaguchi, J., 2011. Analysis of membrane dynamics using multi-particle model for solar sail demonstrator 'IKAROS'. In: 52nd AIAA/ASME/ASCE/AHS/ASC Structures, Structural Dynamics and Materials Conference. Denver, CO., AIAA 2011-1890, https://doi.org/10.2514/6.2011-1890.

Spröwitz, T., Seefeldt, P., Spietz, P., Grundmann, J.T., Jahnke, R., Mikulz, E., Reershemius, S., Renger, T., Sasaki, K., Tóth, N., 2018. Membrane deployment technology development at DLR for solar sails and large-scale photovoltaics. In: IEEE Aerospace Conference. Big Sky, MT, https://doi.org/10.1109/AERO.2019.8741630.

Stylianou, M., Tabarrok, B., 1994. Finite element analysis of an axially moving beam, part I: time integration. J. Sound Vib. 178 (4), 433–453. https://doi.org/10.1006/jsvi.1994.1497.

Stylianou, M., Tabarrok, B., 1994. Finite element analysis of an axially moving beam, part II: stability analysis. J. Sound Vib. 178 (4), 455–481. https://doi.org/10.1006/jsvi.1994.1498.

Stylianou, M.C., 1993. Dynamics of a Flexible Extendible Beam (Ph.D. thesis). University of Victoria, Victoria, BC.

Tabarrok, B., Leech, C.M., Kim, Y.I., 1974. On the dynamics of an axially moving beam. J. Franklin Inst. 297 (3), 201–220. https://doi.org/10.1016/0016-0032(74)90104-5.

Tian, Q., Zhao, J., Liu, C., Zhou, C., 2015. Dynamics of space deployable structures. In: Proceedings of the ASME 2015 International Design Engineering Technical Conferences & Computers and Information in Engineering Conference. Boston, MA., https://doi.org/10.1115/DETC2015-46159

Tisseur, F., Meerbergen, K., 2001. The quadratic eigenvalue problem. SIAM Rev. 43 (2), 235–286. https://doi.org/10.1137/S0036144500381988.

Vatankhahghadim, B., Damaren, C.J., 2018. Solar sail deployment dynamics. In: The Fifth Joint International Conference on Multibody System Dynamics. Lisboa, Portugal.

Vatankhahghadim, B., Damaren, C.J., 2019. Deployment of a membrane attached to two axially moving beams. ASME J. Appl. Mech. 86(3), 031003–(1-12). https://doi.org/10.1115/1.4042134

Wang, L.H., Hu, Z., Zhong, Z., 2010. Dynamic analysis of an axially translating plate with time-variant length. Acta Mech. 215 (1–4), 9–23. https://doi.org/10.1007/s00707-010-0290-0.

Wang, L.H., Hu, Z.D., Zhong, Z., Ju, J.W., 2009. Hamiltonian dynamic analysis of an axially translating beam featuring time-variant velocity. Acta Mech. 206 (3–4), 149–161. https://doi.org/10.1007/s00707-008-0104-9.

Wang, P.K.C., Wei, J.-D., 1987. Vibrations in a moving flexible robot arm. J. Sound Vib. 116 (1), 149–160. https://doi.org/10.1016/S0022-460X(87)81326-3.

Wang, P.K.C., Wei, J.-D., 1994. Correction and remarks on 'vibrations in a moving flexible robot arm'. J. Sound Vib. 172 (3), 413–414. https://doi.org/10.1006/jsvi.1994.1183.

Weeks, G.E., 1986. Dynamic analysis of a deployable space structure. J. Spacecraft Rockets 23 (1), 102–107. https://doi.org/10.2514/3.25090.

Wickert, J.A., Mote Jr., C.D., 1988. Current research on the vibration and stability of axially-moving materials. Shock Vib. Digest 20 (5), 3–13.

Wickert, J.A., Mote Jr., C.D., 1989. On the energetics of axially moving continua. J. Acoust. Soc. Am. 85 (3), 1365–1368. https://doi.org/10.1121/1.397418.

Wickert, J.A., Mote Jr., C.D., 1990. Classical vibration analysis of axially moving continua. ASME J. Appl. Mech. 57 (3), 738–744. https://doi.org/10.1115/1.2897085.

Wong, Y., Pellegrino, S., 2006. Wrinkled membranes. Part I: experiments. J. Mech. Mater. Struct. 1 (1), 3–25. https://doi.org/10.2140/jomms.2006.1.3.

Wu, J., Shao, M., Wang, Y., Wu, Q., Nie, Z., 2017. Nonlinear vibration characteristics and stability of the printing moving membrane. J. Low Frequency Noise Vib. Active Control 36 (3), 306–316. https://doi.org/10.1177/0263092317711597.

Yang, X.-D., Zhang, W., Melnik, R.V.N., 2016. Energetics and invariants of axially deploying beam with uniform velocity. AIAA J. 54 (7), 2181–2187. https://doi.org/10.2514/1.J054383.

Zhang, L., Zu, J.W., 1999. Nonlinear vibration of parametrically excited viscoelastic moving belts, part II: stability analysis. ASME J. Appl. Mech. 66 (2), 403–409. https://doi.org/10.1115/1.2791063.

Zhao, J., Tian, Q., Hu, H.-Y., 2013. Deployment dynamics of a simplified spinning IKAROS solar sail via absolute coordinate based method. Acta. Mech. Sin. 29 (1), 132–142. https://doi.org/10.1007/s10409-013-0002-9.

Zhu, W.D., 2000. Vibration and stability of time-dependent translating media. Shock Vib. Digest 32 (5), 369–379. https://doi.org/10.1177/058310240003200502.

Please cite this article as: B. Vatankhahghadim and C. J. Damaren, Solar sail deployment dynamics, Advances in Space Research, https://doi.org/10.1016/j.asr.2020.03.029

Zhu, W.D., 2002. Control volume and system formulations for translating media and stationary media with moving boundaries. J. Sound Vib. 254 (1), 189–201. https://doi.org/10.1006/jsvi.2001.4055.

Zhu, W.D., Ni, J., 2000. Energetics and stability of translating media with an arbitrarily varying length. J. Vib. Acoust. 122 (3), 295–304. https://doi.org/10.1115/1.1303003.

Ziegler, H., 1956. On the concept of elastic stability. Adv. Appl. Mech. 4, 351–403. https://doi.org/10.1016/S0065-2156(08)70376-4.

Ziegler, H., 1977. Principles of Structural Stability. Birkhäuser Verlag Basel.

Please cite this article as: B. Vatankhahghadim and C. J. Damaren, Solar sail deployment dynamics, Advances in Space Research, https://doi.org/10.1016/j.asr.2020.03.029